

Title No. 121-S05

# Flexural Behavior of Carbon Fiber-Reinforced Polymer Partially Bonded Reinforced Concrete Beams with Different Anchorage Methods

by Qi Cao, Xingchao Wang, Zhimin Wu, Rongxiong Gao, and Xin Jiang

*Carbon fiber-reinforced polymer (CFRP) is a widely used material for reinforced concrete (RC) beam strengthening. Because of exposure to severe environments and improper construction, CFRP sheets may separate from the bottom of RC beams. To analyze the influence of this type of interfacial defect on the mechanical properties of RC beams quantitatively and provide a reference for the rehabilitation of structures, this paper investigates the flexural properties of RC beams strengthened with partially bonded CFRP by experiments and analytical studies. To measure the degree of unbonded CFRP, a new parameter called the unbonded ratio was established, which is defined as the ratio of unbonded length to the total length of strengthening CFRP in the tension zone. Twenty-six RC beams were fabricated and tested in the present study, and the experimental variables were the unbonded ratio, thickness of the CFRP sheet, and anchorage method (vertical U-jacket, inclined U-jacket, and mechanical plate). The cracking load, ultimate load, load-midspan deflection curve, ductility, crack pattern, and failure modes of these specimens are discussed. Also, the coupling effect of the unbonded CFRP and anchorage method on the flexural performance of strengthened beams was investigated. Test results indicated that the ultimate load decreased with the increase of the unbonded ratio before the unbonded ratio reached its critical value. It was also found that the mechanical-plate anchorage and inclined U-jackets were superior to traditional vertical U-jackets in terms of load-carrying capacity and flexural stiffness and postponed the debonding of CFRP. Finally, a theoretical model for the ultimate load of RC beams strengthened with inclined U-jackets was proposed, which showed a good agreement with the test results.*

**Keywords:** anchorage; concrete beam; flexural performance; partially bonded carbon fiber-reinforced polymer (CFRP); unbonded ratio.

## INTRODUCTION

Attributed to the advantages of high strength, low weight, and excellent corrosion resistance, carbon fiber-reinforced polymer (CFRP) is getting more and more attention from researchers, engineers, and project managers. Regarding the external reinforcement by CFRP, researchers have studied the influence of distinct experimental variables on CFRP-strengthened structures, such as the position of CFRP reinforcement, the thickness of the CFRP sheet, and the shape of CFRP reinforcement forms (U-shaped bonding, spaced strip bonding, or the combination of different bonding techniques).<sup>1-5</sup> These studies showed that the application of CFRP reinforcement could postpone the cracking<sup>1</sup> and enhance the structural performance of reinforced concrete (RC) beams.<sup>4</sup>

When the CFRP sheet is employed to enhance the bending strength of the RC beam, researchers often assume that the

perfect bonding can be achieved by using adhesive resins and various anchorages.<sup>6,7</sup> However, due to exposure to severe environments and improper construction methods, the CFRP sheet often separates from an RC beam in its service life, leading to interfacial defects and a change in load-carrying capacity. In this case, the beam strengthened with fully bonded CFRP is converted into a beam strengthened with partially bonded CFRP. Because the delamination between CFRP sheets and the surface of RC beams is difficult to detect, it is necessary to consider the post-debonding load-carrying capacity of the member before strengthening construction to ensure safety during the service life.

Currently, there are few quantitative studies on the mechanical properties of RC beams strengthened with partially bonded CFRP, and researchers' opinions are divided. Zhou et al.<sup>8</sup> argued that partial debonding of CFRP at the pure bending zone will reduce the ultimate load slightly, while debonding at the shear-bending zone will reduce the ultimate load significantly. However, other researchers<sup>9-18</sup> treated partially bonded CFRP as a novel reinforcement system for RC beams. Burgoyne<sup>9</sup> proposed that it was not necessary for FRP to be fully bonded to concrete and suggested an unbonded system for FRP-strengthened beams. Lees and Burgoyne<sup>10,11</sup> investigated the mechanical properties of beams with partially bonded composite reinforcement and concluded that the ultimate load of the partially bonded beams was equivalent to that of fully bonded beams. Chahrouh and Soudki<sup>12</sup> and Choi et al.<sup>13</sup> conducted bending tests on partially bonded CFRP-strengthened RC beams and deduced the analytical expressions for the yield load and ultimate load-carrying capacity through the moment-curvature relationship. In addition, researchers<sup>14-18</sup> observed in their experiments and finite element analyses that partially bonded CFRP leads to increased load-carrying capacity and ductility. Therefore, there are no widely accepted conclusions on how CFRP debonding affects the mechanical properties of RC beams. Perhaps because of the existence of controversy, current codes have a low acceptance of this new reinforcement system and most of them do not address

*ACI Structural Journal*, V. 121, No. 1, January 2024.

MS No. S-2022-402.R1, doi: 10.14359/51739185, received August 14, 2023, and reviewed under Institute publication policies. Copyright © 2024, American Concrete Institute. All rights reserved, including the making of copies unless permission is obtained from the copyright proprietors. Pertinent discussion including author's closure, if any, will be published ten months from this journal's date if the discussion is received within four months of the paper's print publication.

**Table 1—Mixture proportions and compressive strength of concrete**

| Grade | Cement, kg/m <sup>3</sup> (lb/yd <sup>3</sup> ) | Fine aggregate, kg/m <sup>3</sup> (lb/yd <sup>3</sup> ) | Coarse aggregate, kg/m <sup>3</sup> (lb/yd <sup>3</sup> ) | Water, kg/m <sup>3</sup> (lb/yd <sup>3</sup> ) | Compressive strength at 28 days, MPa (ksi) |
|-------|---|---|---|--|--|
| C40   | 450 (759)                                       | 636 (1073)  | 995 (1679)  | 210 (354)                                      | 45.39 (6.58)                               |

the intentionally partially bonded FRP. Instead, they always treat the delamination of FRP as a kind of defect.<sup>19</sup>

Also, studies on the effect of anchorage methods on the mechanical properties of RC beams in the case of partially bonded CFRP have not been reported yet. Anchorages are frequently applied to RC beams strengthened with CFRP sheets. The application of anchorages is intended to prevent CFRP from debonding from the surface of the beam or to delay the delamination and increase the load-carrying capacity. CFRP U-jackets are one of the most widespread anchorage methods that can offer resistance against plate-end debonding. Mechanical plates with bolts are also widely used to improve the load-carrying capacity.<sup>20</sup> In addition to the traditional anchorage methods, researchers also focused on innovative anchorage methods in recent years, such as FRP bar and FRP U-jacket composite anchorages,<sup>21</sup> anchored holes,<sup>22</sup> fiber anchor spikes,<sup>23</sup> mechanical end anchorages,<sup>24</sup> warp and woof straps,<sup>25</sup> and inclined FRP U-jackets,<sup>4,26</sup> most of which improved the load-carrying capacity or serviceability of strengthened structures. Also, by using new grooving techniques for CFRP sheets such as externally bonded reinforcement on grooves (EBROG) and externally bonded reinforcement in grooves (EBRIG), the debonding between the CFRP sheet and concrete substrate can also be delayed,<sup>27-32</sup> with higher load-carrying capacity than reference beams. However, inconvenient construction and high costs hinder the wide application of these anchorage or grooving methods. Furthermore, studies<sup>4,20-26</sup> assumed that CFRP sheets were perfectly bonded to the RC beams and did not take the debonding between CFRP and the concrete substrate into account.

To investigate the combined effects of partially bonded CFRP and anchorage methods on the mechanical properties of RC beams strengthened with CFRP, this study investigated the flexural behavior of RC beams with partially bonded CFRP and three different anchorage methods—that is, vertical U-jacket, mechanical plate, and inclined U-jacket. To measure the degree of unbonded CFRP, a new parameter called the unbonded ratio is proposed, which is defined as the ratio of unbonded length to the total length of strengthening CFRP in the tension zone and denoted as  $\xi$ . The ultimate load, cracking load, flexural stiffness, ductility, crack pattern, and failure mode were studied and analyzed. In the end, a theoretical model to evaluate the ultimate load of RC beams with U-jacket anchorages was proposed. The results of the proposed model showed good agreement with the collected test results in the literature.

## RESEARCH SIGNIFICANCE

Existing research on RC beams strengthened with partially bonded CFRP does not take various anchorage methods into account. The present study aims to investigate the collaborative performance of the partially bonded

CFRP sheet and different anchorage methods and proposes a theoretical model to evaluate the ultimate load of RC beams with U-jacket anchorages. The research achievements of the present study will help to select a suitable anchorage method, estimate the influence of CFRP debonding, and determine whether further repairs are needed.

## EXPERIMENTAL PROCEDURE

### Materials

The concrete mixture proportions were adopted from a previous study.<sup>33</sup> The components of the mixture were ordinary portland cement, river sand, and 5 to 10 mm (0.2 to 0.4 in.) well-graded coarse aggregate. The mixture proportions and 28-day compressive strength are shown in Table 1. The specimen size for the compressive strength test was 150 x 150 x 150 mm (5.9 x 5.9 x 5.9 in.) according to GB/T 50081-2019.<sup>34</sup> The one-layer CFRP sheet had a thickness of 0.167 mm (0.0065 in.), tensile strength of 3400 MPa (493 ksi), elastic modulus of 244 GPa (35,390 ksi), and ultimate strain of 0.014, in which the mechanical properties were obtained from tests according to GB/T 3354-1999.<sup>35</sup> The nominal yield strength of longitudinal steel bars and stirrups were 400 and 300 MPa (58 and 44 ksi), respectively, and the test yield strength of longitudinal bars was 467 MPa (68 ksi), according to GB/T 228.1-2010.<sup>36</sup> The elastic modulus of steel reinforcement was assumed to be 200 GPa (29,000 ksi).

### Specimens

A total of 26 RC beams—including six fully bonded CFRP-strengthened beams, 18 partially bonded CFRP-strengthened beams, and two beams without external CFRP—were fabricated in this experiment. Three anchorage methods were selected for this paper, namely CFRP vertical U-jackets, mechanical plates, and CFRP inclined U-jackets as suggested by Fu et al.<sup>4,26</sup>

The dimensions of the specimens were 1000 x 80 x 120 mm (39.4 x 3.1 x 4.7 in.) and the length of the CFRP sheet was 800 mm (31.5 in.). The details of the specimens are shown in Table 2. The unbonded ratio, which is denoted as  $\xi$ , is defined as the ratio of unbonded length to the total length of CFRP sheet—that is,  $x/L_f$  in Fig. 1. “WB,” “FB,” and “PB” indicate specimens without bonded CFRP, with fully bonded CFRP, and with partially bonded CFRP, respectively. The number after “PB” indicates the percentage form of the unbonded ratio; for example, “010” stands for  $\xi = 10\% = 0.1$ . The number after the hyphen is the number of CFRP layers. The last letters “V,” “I,” and “M” indicate vertical U-jacket, inclined U-jacket, and mechanical plate, respectively.

The details of the reinforcement cages are shown in Fig. 2. Reinforcement cages were placed in wooden molds, then concrete was placed into the formwork and cured for at least 28 days before the beam bending test.

Before attaching the CFRP sheets to the bottom of the beams, the surface of the concrete beam was ground with an angle grinder, followed by a secondary cleaning with sandpaper. Polyethylene terephthalate (PET) was used to keep concrete separate from the CFRP in the unbonded area. This procedure was intended to simulate the interfacial defect of the CFRP bonding.

**Table 2—Details of specimens**

| Specimen | Anchorage method | CFRP layers | Thickness of CFRP sheet, mm | Unbonded ratio | Unbonded length, mm |
|----------|------------------|-------------|-----------------------------|----------------|---------------------|
| WB1      | —                | —           | —                           | —              | —                   |
| WB2      | —                | —           | —                           | —              | —                   |
| FB-1V    | VU               | 1           | 0.167                       | 0              | 0                   |
| FB-1I    | IU               | 1           | 0.167                       | 0              | 0                   |
| FB-1M    | MP               | 1           | 0.167                       | 0              | 0                   |
| FB-2V    | VU               | 2           | 0.334                       | 0              | 0                   |
| FB-2I    | IU               | 2           | 0.334                       | 0              | 0                   |
| FB-2M    | MP               | 2           | 0.334                       | 0              | 0                   |
| PB010-1V | VU               | 1           | 0.167                       | 0.1            | 80                  |
| PB010-1I | IU               | 1           | 0.167                       | 0.1            | 80                  |
| PB010-1M | MP               | 1           | 0.167                       | 0.1            | 80                  |
| PB010-2V | VU               | 2           | 0.334                       | 0.1            | 80                  |
| PB010-2I | IU               | 2           | 0.334                       | 0.1            | 80                  |
| PB010-2M | MP               | 2           | 0.334                       | 0.1            | 80                  |
| PB020-1V | VU               | 1           | 0.167                       | 0.2            | 160                 |
| PB020-1I | IU               | 1           | 0.167                       | 0.2            | 160                 |
| PB020-1M | MP               | 1           | 0.167                       | 0.2            | 160                 |
| PB020-2V | VU               | 2           | 0.334                       | 0.2            | 160                 |
| PB020-2I | IU               | 2           | 0.334                       | 0.2            | 160                 |
| PB020-2M | MP               | 2           | 0.334                       | 0.2            | 160                 |
| PB030-1V | VU               | 1           | 0.167                       | 0.3            | 240                 |
| PB030-1I | IU               | 1           | 0.167                       | 0.3            | 240                 |
| PB030-1M | MP               | 1           | 0.167                       | 0.3            | 240                 |
| PB030-2V | VU               | 2           | 0.334                       | 0.3            | 240                 |
| PB030-2I | IU               | 2           | 0.334                       | 0.3            | 240                 |
| PB030-2M | MP               | 2           | 0.334                       | 0.3            | 240                 |

Note: VU is vertical U-jacket; IU is inclined U-jacket; and MP is mechanical plate. 1 mm = 0.039 in.

As previously mentioned, in the present study, three anchorage methods were considered—namely, vertical U-jackets, inclined U-jackets, and mechanical plates. The details of the three anchorage methods are shown in Fig. 3. It should be noted that the widths of each anchorage are equal, as are the distances between anchorage edges and the ends of the CFRP sheet.

### Four-point bending test

After 7 days of curing of epoxy resin, the four-point bending test was conducted on a 5000 kN (1124.04 kip) hydraulic testing machine. The schematic diagram of the beam test setup is shown in Fig. 4. Figure 5 displays the experimental setup prior to loading for the typical strengthened beam specimens implemented with the three anchorage methods (vertical U-jacket, inclined U-jacket, and mechanical plate). The loading speed was 0.2 mm/min (0.008 in./min). A 200 kN (44.96 kip) load cell was used to measure the loading force. Three displacement sensors were applied to measure the deflection of the beam, one of which was used to measure the midspan deflection, and the other two were applied to measure support deflections.

During the test process, loading was sustained at every 5 kN (1.12 kip), the crack initiation and propagation were marked on one side of the beam, and the crack width was measured with a device that measures the crack width and the microcosmic defects on the concrete surface.

## EXPERIMENTAL RESULTS AND ANALYSIS

### Failure modes

The test results, including cracking load, ultimate load, failure mode, and damage of jacket anchorage, are summarized in Table 3 for reference. Four typical failure modes were observed during the test: concrete crushing, CFRP rupture, plate-end debonding, and intermediate crack debonding.

**Concrete crushing**—Concrete crushing is the typical failure mode of RC beams without externally bonded CFRP, as shown in Fig. 6(a). After yielding of the tensile reinforcement, the depth of the compression zone decreased with increasing applied load, and the concrete in the compression zone at the midspan was eventually crushed. The CFRP sheet might also separate from the bottom of the beam at the time of failure.

**CFRP rupture**—Figure 6(b) shows a typical CFRP rupture failure. The overall debonding of the CFRP was delayed due to the horizontal restraining force provided by the mechanical plate. As a result, the CFRP sheet could reach its ultimate strain and then ruptured with a loud sound. It is noteworthy

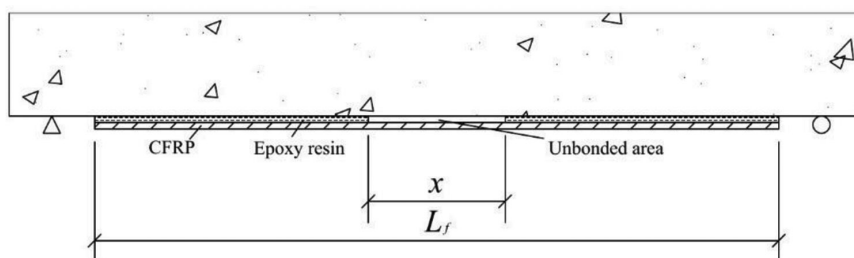


Fig. 1—Concrete beam with partially bonded CFRP.

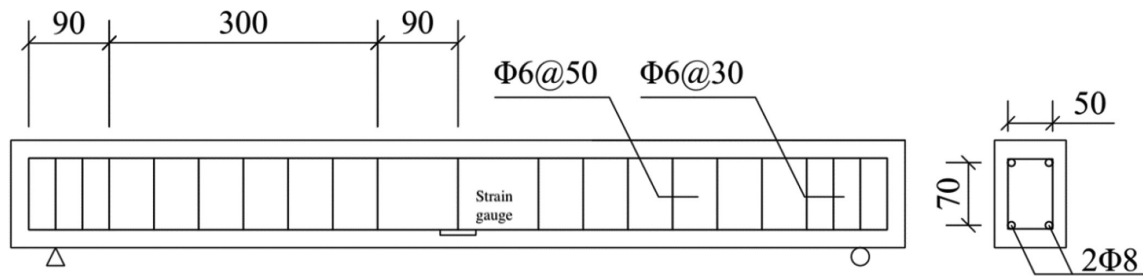


Fig. 2—Reinforcement of test beams. (Note: Units in mm; 1 mm = 0.039 in.)

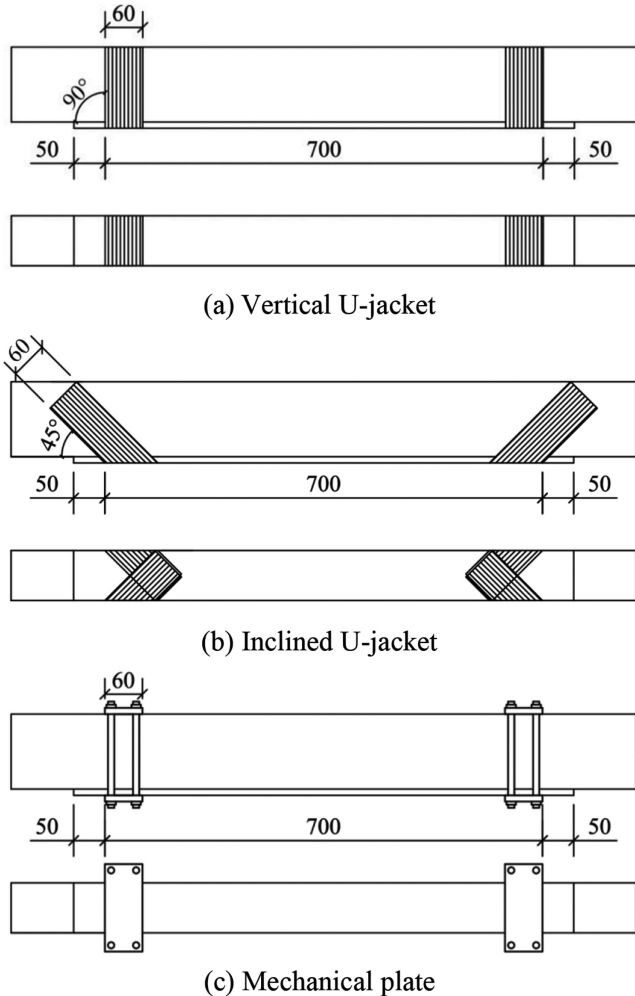


Fig. 3—Schematic diagrams of anchorage methods. (Note: Units in mm; 1 mm = 0.039 in.)

that only half of the CFRP sheet broke with a smooth cross section, while the other half remained almost intact. The reason for this may be due to the uneven stress distribution inside the CFRP sheet.

**Plate-end debonding**—Figure 6(c) exhibits a typical plate-end debonding failure. It can be seen that local stress concentration at the end of the CFRP sheet induced wide shear cracks on the two-layer specimens with vertical U-jackets. With the increase in applied load, the cracks near the inner side of the U-jacket developed rapidly, and small and dense cracks appeared around it. At the time of failure, a bulk of concrete between two major shear cracks was torn off from the bottom of the beam at the end of the CFRP sheet.

Table 3—Experimental results

| Specimen | Cracking load $P_{cr}$ , kN | Ultimate load $P_{us}$ , kN | Failure mode | Jacket anchorage damage |
|----------|-----------------------------|-----------------------------|--------------|-------------------------|
| WB1      | 2.3                         | 29.7                        | CC           | N/A                     |
| WB2      | 2.5                         | 27.7                        | CC           | N/A                     |
| FB-1V    | 4.2                         | 42.7                        | IC           | R                       |
| FB-1I*   | —                           | 51.6                        | IC           | N                       |
| FB-1M    | 5.6                         | 49.5                        | CC+IC        | N/A                     |
| FB-2V    | 6.1                         | 44.5                        | PE           | N                       |
| FB-2I    | 6.3                         | 56.9                        | IC           | R                       |
| FB-2M    | 6.2                         | 57.8                        | IC           | N/A                     |
| PB010-1V | 4.0                         | 44.4                        | IC           | N                       |
| PB010-1I | 3.9                         | 47.6                        | IC           | D                       |
| PB010-1M | 4.4                         | 49.0                        | IC           | N/A                     |
| PB010-2V | 6.1                         | 44.2                        | PE           | D                       |
| PB010-2I | 5.7                         | 50.5                        | IC           | N                       |
| PB010-2M | 6.3                         | 54.3                        | IC           | N/A                     |
| PB020-1V | 3.7                         | 44.6                        | IC           | R                       |
| PB020-1I | 4.7                         | 49.6                        | CC+IC        | N                       |
| PB020-1M | 4.3                         | 47.9                        | CR           | N/A                     |
| PB020-2V | 6.2                         | 47.3                        | PE           | N                       |
| PB020-2I | 5.9                         | 54.0                        | IC           | R                       |
| PB020-2M | 5.3                         | 60.4                        | CC+IC        | N/A                     |
| PB030-1V | 4.5                         | 44.8                        | IC           | N                       |
| PB030-1I | 4.0                         | 48.8                        | CC+IC        | N                       |
| PB030-1M | 4.2                         | 44.4                        | IC           | N/A                     |
| PB030-2V | 6.5                         | 44.8                        | PE           | N                       |
| PB030-2I | 5.6                         | 52.4                        | IC           | D                       |
| PB030-2M | 6.2                         | 63.5                        | IC           | N/A                     |

\*The cracking load of FB-1I is not accessible due to misoperation, which applied impact load on the specimen during the test.

Note: CC is concrete crushing; IC is intermediate crack debonding; PE is plate-end debonding; CR is CFRP rupture; R is U-jacket rupture; D is U-jacket debonding; N is no damage; and N/A is not applicable. 1 kN = 0.225 kip.

**Intermediate crack (IC) debonding**—IC debonding was the main failure mode of the test, which is shown in Fig. 6(d). After yielding of the tensile reinforcement, the CFRP sheet at the bottom of the beam made tearing sounds occasionally. Then, the tearing sound was heard continuously for a few seconds before the CFRP separated from the beam. After

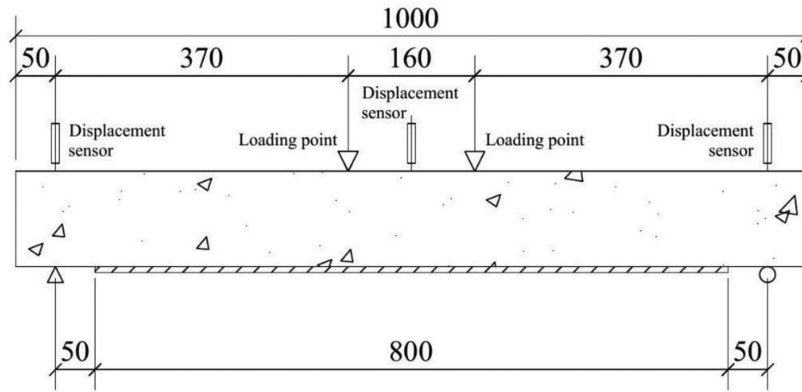
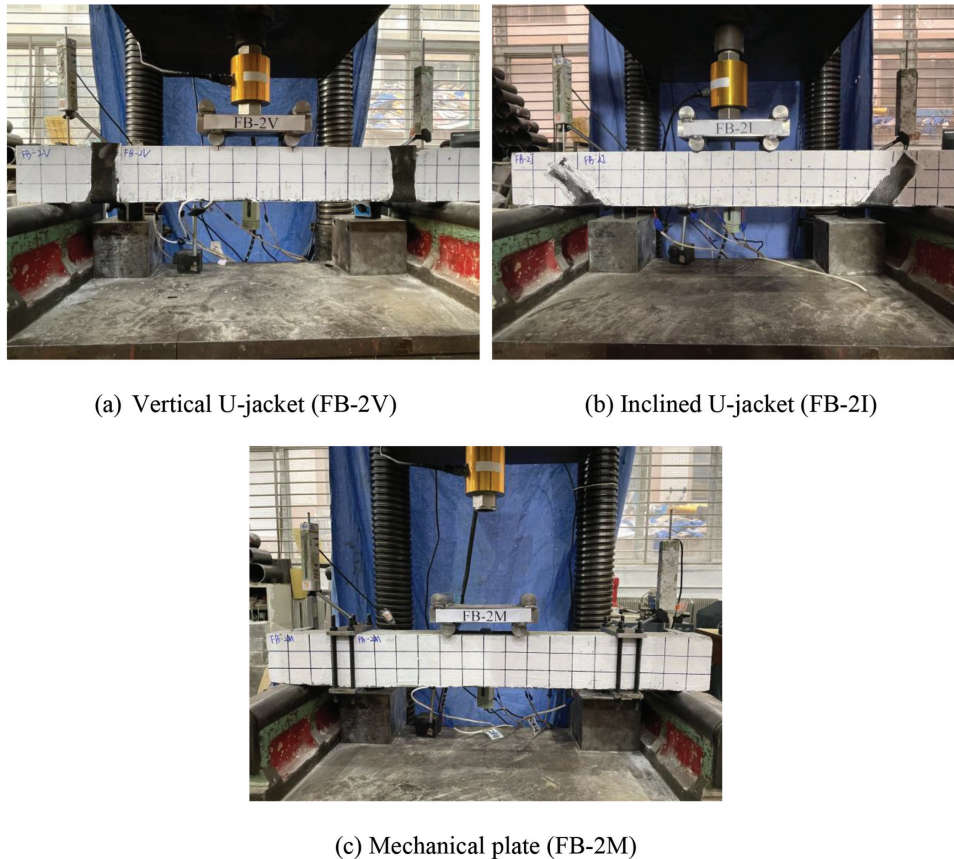


Fig. 4—Schematic diagram of beam test setup. (Note: Units in mm; 1 mm = 0.039 in.)



(a) Vertical U-jacket (FB-2V)

(b) Inclined U-jacket (FB-2I)

(c) Mechanical plate (FB-2M)

Fig. 5—Beam test setup prior to loading.

that, the debonding of the CFRP occurred near the midspan of the specimen with a loud noise. The CFRP sheet was observed to be split into several thin strips due to the sudden release of great energy during the debonding process. The main body of the beam was still able to carry the applied load after debonding and finally failed by crushing of the concrete. According to Teng and Chen,<sup>37</sup> IC debonding is induced by local interfacial stress near the cracks. Because there is a singularity and concentration in the stress distribution at the unbonded boundary, IC tends to occur from cracks near the unbonded boundary.

Depending on the pattern of the CFRP U-jacket at the time of failure, IC debonding could be subdivided into three classes: CFRP jacket rupture, CFRP jacket debonding, and

debonding without additional damage to the jacket. The corresponding specimens are listed in Table 3.

Damage to the CFRP jacket was induced by the released energy caused during the debonding of the CFRP sheet at the bottom of the beam, and the specific damage form depended on the shear strength of the concrete-epoxy resin interfacial adhesive layer, the tensile strength of CFRP, and the magnitude of the energy. When the shear strength of the concrete-epoxy resin interfacial adhesive layer was sufficient to resist released energy, but the tensile strength of CFRP was not sufficient, the CFRP jacket rupture would occur, as shown in Fig. 7(a). If the aforementioned condition was reversed, then CFRP jacket debonding would occur, as demonstrated in Fig. 7(b). If each strength was sufficient to withstand the released energy, then the anchorage would remain

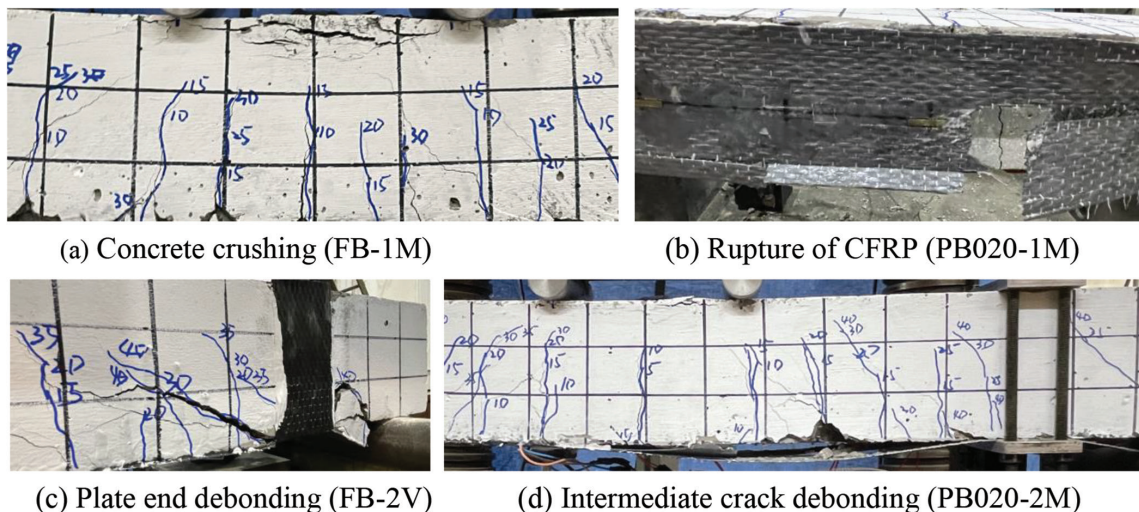


Fig. 6—Failure modes.

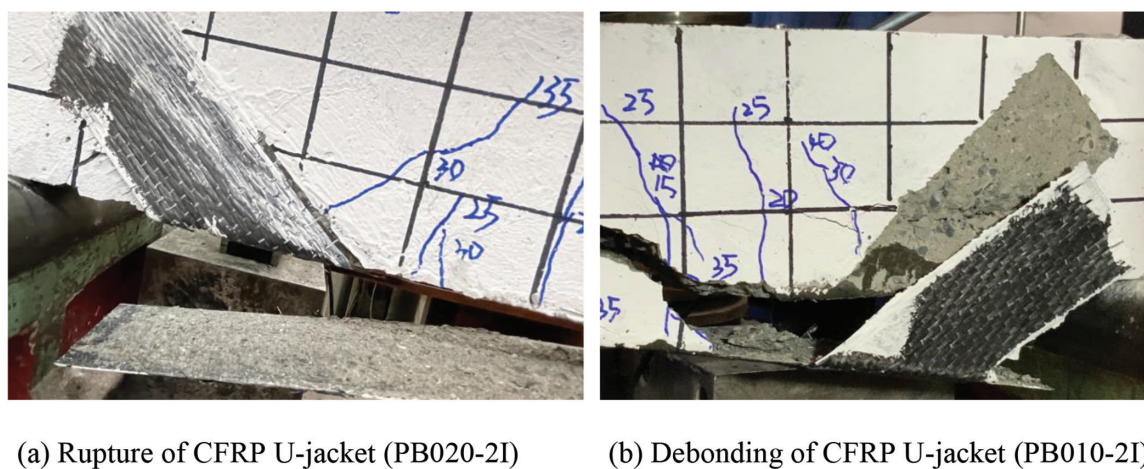


Fig. 7—Damage of CFRP U-jacket.

undamaged. This brittle damage does not occur when using mechanical plates because the concrete-epoxy resin layer was not applied. This is one advantage of the mechanical plates over the CFRP U-jacket anchorage methods.

### Crack patterns and propagation

The propagation of cracks was marked and recorded during the test. It should be noted that the initial crack was formed on FB-II, on which the impact load was applied due to mishandling. The recorded crack width of FB-II was measured during the second loading process.

The load-maximum crack width curves ( $P-w_{cr}$  curves) of the specimens with the same unbonded ratios are shown in Fig. 8. It can be seen that when the same anchoring method is used, the cracks in the two-layer specimens are smaller than those in the one-layer specimens, regardless of the unbonded ratios. In addition, the anchorage method did not exhibit a significant effect on the crack width of the specimens.

The relationships between  $P$  and  $w_{cr}$  under the condition of the same anchorage method are shown in Fig. 9. In the case of using vertical U-jackets and mechanical plates, the FB specimens had the smallest  $w_{cr}$  regardless of the thickness of the CFRP. For specimens using inclined U-jackets,

PB030-II had the smallest  $w_{cr}$  among the one-layer specimens, while FB-II and PB010-2I had the smallest  $w_{cr}$  in the early and late stages of the loading process, respectively. In general, fully bonded CFRP sheets were most effective in restraining crack propagation.

It should be noted that the crack width  $w_{cr}$  mentioned here refers to the width of the flexural or flexural-shear crack between two anchorages. The crack patterns of the PB010 specimens are shown in Fig. 10 as typical, and other specimens are similar to these.

### Cracking load and ultimate load

Experimental results of cracking load are shown in Table 3 and Fig. 11(a).

It can be indicated that the cracking load was not significantly affected by the anchorage method and the unbonded ratio  $\xi$ . Prior to the cracking in the tensile region of the concrete beam, the deformation of the concrete surface and CFRP sheets was highly concentrated in the vicinity of the midspan, and anchorage had not worked effectively yet.

It is further exhibited in Fig. 11(a) that the number of CFRP layers was the only variable that had a significant effect on the cracking load. The average cracking loads of

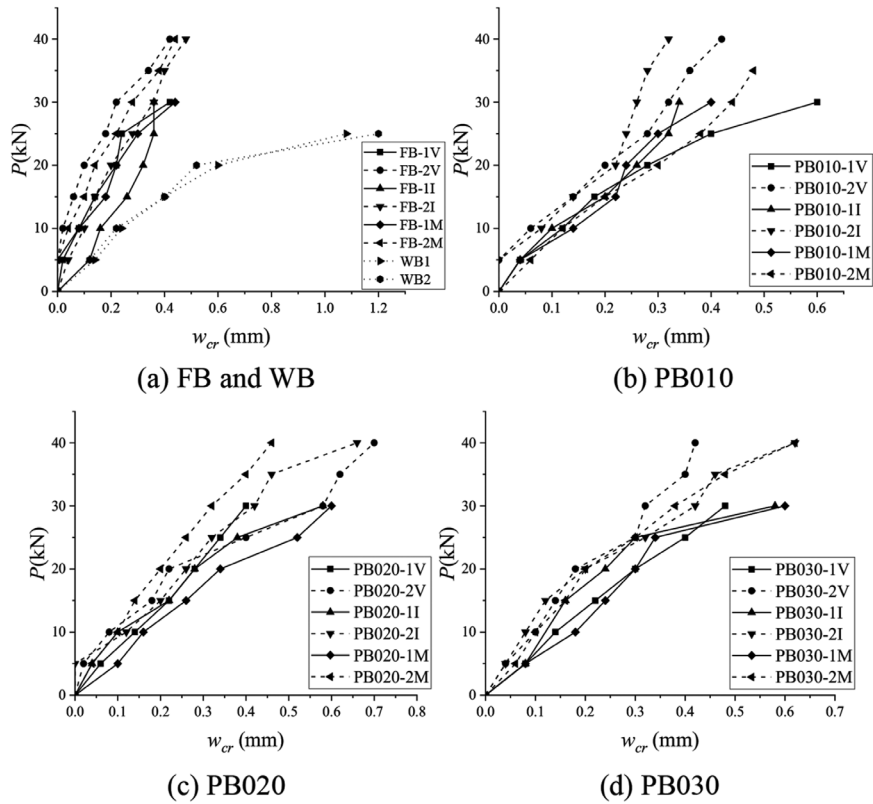


Fig. 8—Load-maximum crack width curves (same unbonded ratio). (Note: 1 kN = 0.225 kip; 1 mm = 0.039 in.)

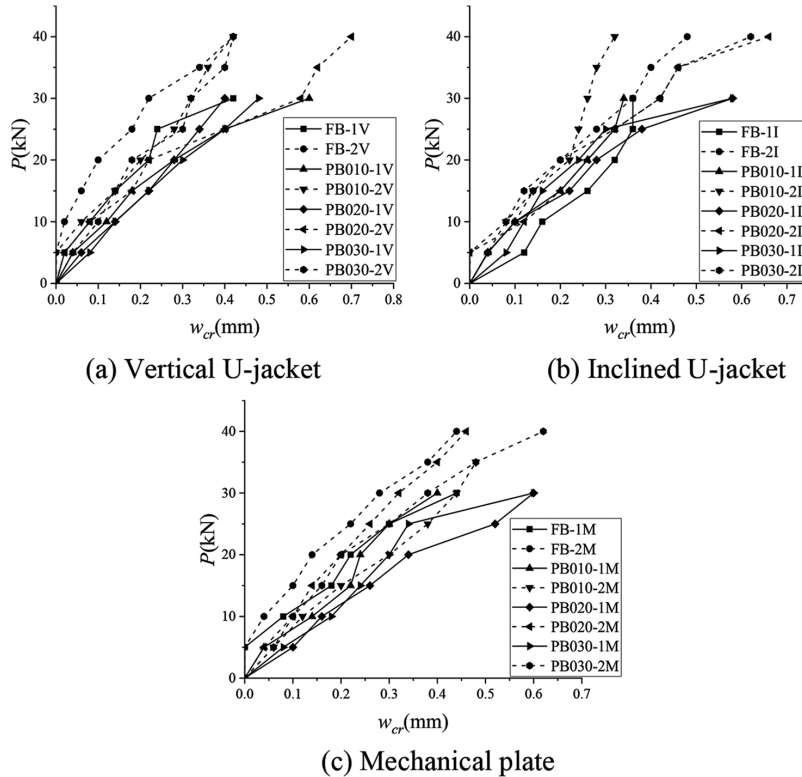


Fig. 9—Load-maximum crack width curves (same anchorage method). (Note: 1 kN = 0.225 kip; 1 mm = 0.039 in.)

zero (WB specimens), one, and two CFRP layer(s) were 2.4, 4.3, and 6.0 kN (0.52, 0.97, and 1.35 kip), respectively. Hence, the cracking loads of beam specimens increased with the number of CFRP layers.

Experimental results of ultimate loads are shown in Table 3 and Fig. 11(b).

First, the effect of the unbonded ratio  $\xi$  on the ultimate load  $P_u$  was considered. In the 1I, 2I, and 1M series, the maximum  $P_u$  occurred on the FB specimen in series 1I, 2I,



Fig. 10—Crack patterns of PB010 series.

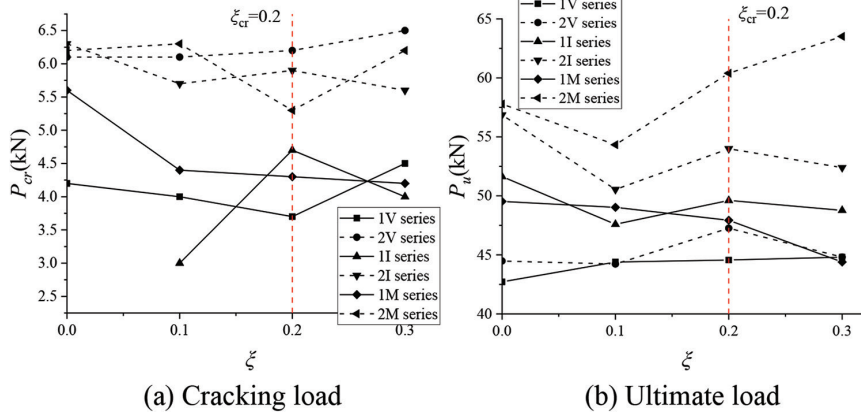


Fig. 11—Relationship between cracking (ultimate) load and unbonded ratio. (Note: 1 kN = 0.225 kip.)

and 1M. However, in series 1V, 2V, and 2M, the maximum  $P_u$  occurred on PB030-1V, PB020-2V, and PB030-2M, respectively, which were 15.0, 17.6, and 19.7% higher than those of the FB specimens.

It can be seen that  $P_u$  decreased as  $\xi$  increased from 0 to 0.1, except for series 1V. Figure 11(b) also shows that  $P_u$  increased when  $\xi$  increased from 0.1 to 0.2, except for series 1M. Note that the length of the pure bending zone  $L_{pb}$  and length of the CFRP sheet  $L_f$  were 160 and 800 mm (6.3 and 31.5 in.), respectively, while the abnormal improvement of  $P_u$  occurred when  $\xi = L_{pb}/L_f = 0.2$ . Therefore,  $\xi = L_{pb}/L_f$  is defined as the critical unbonded ratio and is denoted as  $\xi_{cr}$ . It can be concluded that  $P_u$  decreases with  $\xi$  until  $\xi$  reaches  $\xi_{cr}$  and increases with  $\xi$  as  $\xi$  approaches  $\xi_{cr}$ .

When  $\xi$  increased from 0.2 to 0.3,  $P_u$  increased for the four series 1I, 1M, 2V, and 2I and decreased for the two series 1V and 2M. Therefore, no general conclusion can be determined for  $P_u$  when  $\xi$  exceeds  $\xi_{cr}$ .

Meanwhile,  $P_u$  of the two-layer CFRP specimens were higher than those of the one-layer CFRP specimens. However,  $P_u$  of the 2V series were not significantly higher than those of the 1V series. Different from vertical U-jackets,  $P_u$  of the 2I and 2M series were significantly higher than those of the corresponding one-layer series. Besides, both the inclined U-jacket and mechanical-plate specimens had higher  $P_u$  than the vertical U-jacket specimens. Because IC debonding is induced by local interfacial stress near the cracks according to Teng and Chen,<sup>37</sup> appropriate horizontal forces can postpone the occurrence of IC debonding by mitigating the local

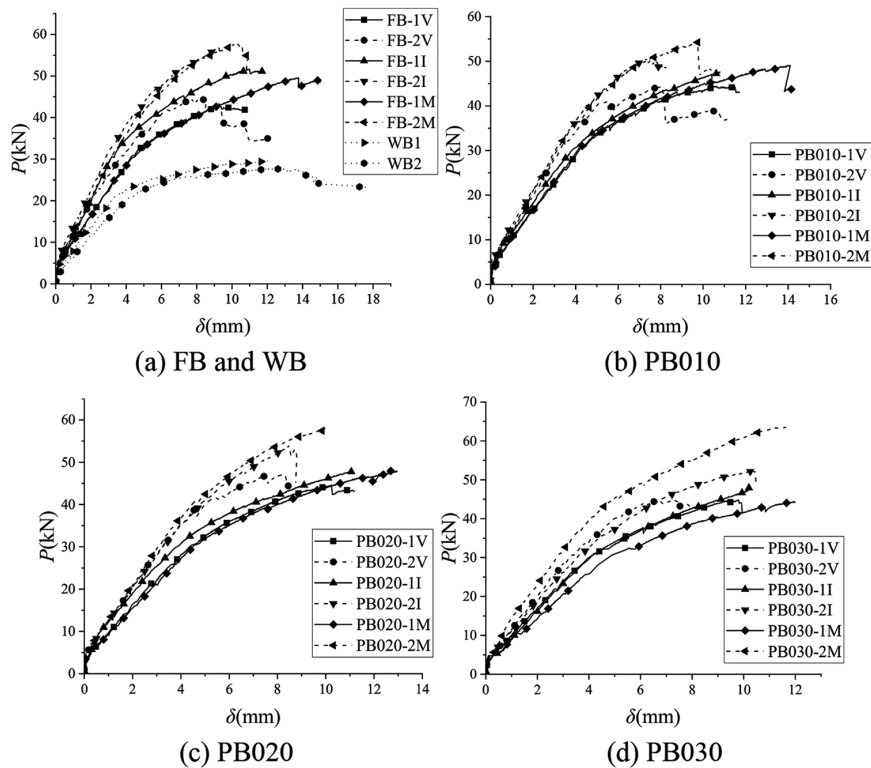


Fig. 12—Load-midspan deflection curves (same unbonded ratio). (Note: 1 kN = 0.225 kip; 1 mm = 0.039 in.)

interfacial stress. Inclined U-jackets and mechanical plates could provide horizontal force through decomposition of the oblique force and friction, respectively, resulting in higher  $\epsilon_{fd}$  (debonding strain of CFRP) and thus higher  $P_u$ . Also, if the increased amount of  $\epsilon_{fd}$  is assumed to be independent of  $t_f$  (thickness of CFRP), then  $P_u$  significantly increases with  $t_f$  because  $P_u$  is positively correlated with  $\epsilon_{fd}t_f$ . In addition,  $P_u$  of the 2M series were higher than those of the 2I series, suggesting that the mechanical plates could postpone the occurrence of IC debonding more effectively than inclined U-jackets. The abnormal increase in  $P_u$  at  $\xi_{cr}$  can also be explained by the theory by Teng and Chen. The increase in individual  $\xi$  tends to decrease  $P_u$ . However, crack widths are larger at midspan in general, and the local interfacial stresses are also larger. The increase in  $\xi$  leads to the possibility that the bonded part avoids large cracks, thereby delaying the onset of IC debonding and increasing the  $P_u$ . These two effects together determine the  $P_u$ . For  $\xi = 0.1$ , the bonded area might not have avoided large cracks, which led to lower  $P_u$ . For  $\xi = \xi_{cr} = 0.2$ , the unbonded area was large enough so that the large cracks would not appear in the bonded area. Therefore, the combined effects result in higher  $P_u$ . Finally, for  $\xi = 0.3$ , there was no significant reduction in crack width at the bonded area, so the effect from the reduction in the unbonded ratio dominated again, leading to a lower  $P_u$ .

### Load-midspan deflection curves

The load-midspan deflection curves ( $P$ - $\delta$  curves) under the condition of the same unbonded ratio are shown in Fig. 12.

For the FB series, it is indicated from Fig. 12(a) that the stiffness of the two-layer specimens was higher than that of one-layer specimens in the early stages of loading. The stiffness was similar among specimens with the same number

of CFRP layers. The stiffness of all specimens decreased with increasing load, and the one-layer specimens decreased more rapidly than the two-layer specimens, which resulted in lower  $P_u$  for FB-1I than for FB-2I and FB-2M. Also, as the load increased, the longitudinal reinforcement yielded and the stiffness of FB-1I increased relative to other specimens, which was close to that of FB-2I and FB-2M, while the stiffness of FB-2V decreased relative to other specimens. Thus, the stiffness of FB-1I eventually exceeded that of FB-2V.

For the PB010 series, it is indicated from Fig. 12(b) that PB010-1I had the highest stiffness among the one-layer specimens, while PB-2V had the lowest stiffness among the two-layer specimens, which was similar to the FB series.

For the PB020 series, it is shown in Fig. 12(c) that the stiffness of PB020-1I was close to that of the two-layer specimens in the early stages of loading. As the reinforcement yielded, the stiffness of PB020-1I decreased and tended to approach the stiffness of the other two one-layer specimens. The stiffness of the two-layer specimens was almost equal because the curves of the different specimens were almost coincident.

It is shown in Fig. 12(d) that the  $P$ - $\delta$  curves of the PB030 series are significantly distinct from those of the other series. First, two specimens with mechanical plates, namely PB030-1M and PB030-2M, exhibited a significant relative decrease and increase in stiffness among the one-layer specimens and two-layer specimens, respectively. Second, the stiffness of the vertical U-jacket and inclined U-jacket specimens did not show significant differences in the PB030 series, while the stiffness of the inclined U-jacket specimens was higher than that of the vertical U-jacket specimens in the other series.

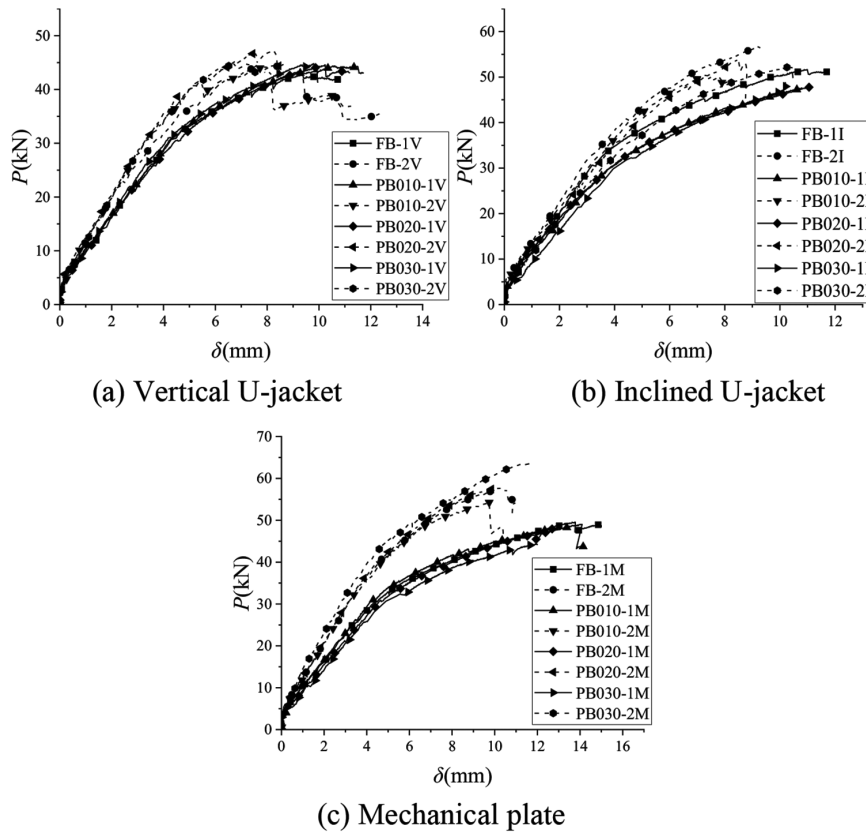


Fig. 13—Load-midspan deflection curves (same anchorage method). (Note: 1 kN = 0.225 kip; 1 mm = 0.039 in.)

Based on the previous analysis, it can be inferred that the inclined U-jacket could significantly improve the stiffness of the RC beam with the best performance. The stiffness of specimens with mechanical plates was higher than that of specimens with vertical U-jackets.

Relations of  $P$  and  $\delta$  under the condition of the same anchorage methods are shown in Fig. 13. It is indicated from Fig. 13 that  $\xi$  had little effect on the stiffness of specimens. In general, the stiffness of the two-layer specimens was higher than that of the one-layer specimens. Besides, the number of CFRP layers and the anchorage method had coupled effects in enhancing the stiffness. The difference in stiffness between the two- and one-layer specimens using mechanical plates was higher than that of the specimens using the two U-jacket anchorage methods. It showed that the mechanical plates performed much better with the thicker CFRP based on experimental results of ultimate load and stiffness.

### Ductility

In general, the ductility of concrete beams can be assessed by the displacement ductility index, which is calculated by dividing the ultimate displacement  $\delta_u$  by the yield displacement  $\delta_y$ —namely,  $\eta_D = \delta_u/\delta_y$ . Because the specimens in the present study were RC beams strengthened with CFRP sheets,  $\delta_y$  derived from the yielding of reinforcement could not express the ductility of the whole member. Park<sup>38</sup> suggested that  $\delta_y$  for concrete structures could be chosen as the intersection of the straight line  $y = P_u$  with the line determined by the original point and  $0.75P_u$  point on the  $P$ - $\delta$  curve.  $\delta_u$  is chosen as the midspan displacement at the time

of failure of the specimen. The definitions of  $\delta_y$  and  $\delta_u$  are illustrated in Fig. 14(a).

The calculated  $\eta_D$  and all related data are listed in Table 4, and the relationship between the displacement ductility index and unbonded ratio is shown in Fig. 14(b).

As shown in Fig. 12, the  $P$ - $\delta$  curves of the specimens strengthened with CFRP sheets do not have significant yield platforms due to CFRP debonding, which is a type of brittle failure. Therefore, the ductility of these specimens is very low. Figure 14(b) indicates that the ductility of the one-layer specimens decreased significantly with the increase in the unbonded ratio  $\xi$ . For the two-layer specimens, the ductility of the 2V series did not change significantly with increasing  $\xi$ , while the ductility of the 2I and 2M series increased first, then decreased, and finally increased as  $\xi$  increased from 0 to 0.3. Meanwhile, it is also exhibited in Fig. 14(b) that the ductility of PB030-2I and PB030-2M were approximately equal to those of FB-2I and FB-2M, respectively.

Under the conditions of the same anchorage method and unbonded ratio, Fig. 14(b) shows that the one-layer specimens exhibited higher ductility than the two-layer specimens. This can be explained by the fact that CFRP is a linear-elastic material and does not contribute much ductility to the strengthened beam, which is mainly provided by the steel reinforcement. For this reason, the higher strengthening ratio of CFRP reduced the ductility of the beams.

With the same CFRP thickness and unbonded ratio, overall, the highest ductility was observed for the vertical U-jacket specimens, while the lowest ductility was observed for the inclined U-jacket specimens. This result is in good agreement with the study by Fu et al.<sup>4</sup> However, it was found

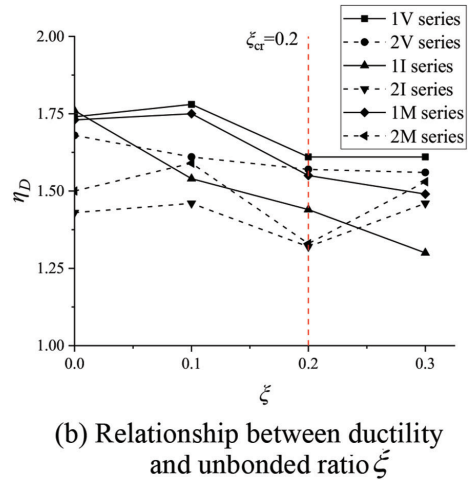
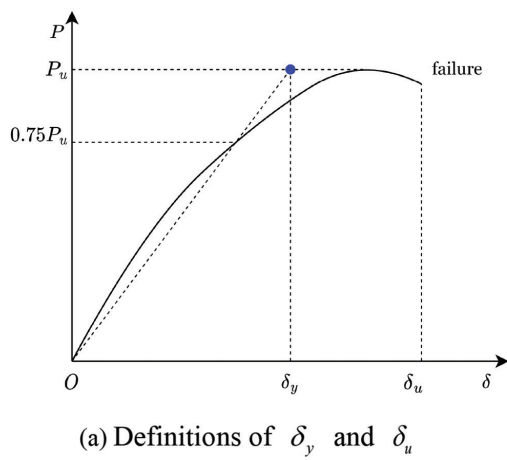


Fig. 14—Displacement ductility index: definition and its relationship to unbonded ratio  $\xi$ .

Table 4—Displacement ductility indexes of specimens

| Specimen | $P_y$ , kN | $\delta_y$ , mm | $\delta_u$ , mm | $\eta_D$ |
|----------|------------|-----------------|-----------------|----------|
| FB-1V    | 36.7       | 6.20            | 10.81           | 1.74     |
| FB-1I    | 43.8       | 6.70            | 11.77           | 1.76     |
| FB-1M    | 41.8       | 8.68            | 15.00           | 1.73     |
| FB-2V    | 39.6       | 5.73            | 9.61            | 1.68     |
| FB-2I    | 49.5       | 6.50            | 9.30            | 1.43     |
| FB-2M    | 51.0       | 7.21            | 10.84           | 1.50     |
| PB010-1V | 37.7       | 6.60            | 11.72           | 1.78     |
| PB010-1I | 40.9       | 7.03            | 10.81           | 1.54     |
| PB010-1M | 41.8       | 8.04            | 14.10           | 1.75     |
| PB010-2V | 40.6       | 5.08            | 8.18            | 1.61     |
| PB010-2I | 44.9       | 5.64            | 8.26            | 1.46     |
| PB010-2M | 47.8       | 6.52            | 10.37           | 1.59     |
| PB020-1V | 38.4       | 6.97            | 11.19           | 1.61     |
| PB020-1I | 41.5       | 7.67            | 11.08           | 1.44     |
| PB020-1M | 40.9       | 8.34            | 12.95           | 1.55     |
| PB020-2V | 40.6       | 5.50            | 8.64            | 1.57     |
| PB020-2I | 47.3       | 6.69            | 8.80            | 1.32     |
| PB020-2M | 52.6       | 7.51            | 9.96            | 1.33     |
| PB030-1V | 38.5       | 6.54            | 10.56           | 1.61     |
| PB030-1I | 42.4       | 7.87            | 10.21           | 1.30     |
| PB030-1M | 38.8       | 8.07            | 12.01           | 1.49     |
| PB030-2V | 40.3       | 5.08            | 7.91            | 1.56     |
| PB030-2I | 46.2       | 7.19            | 10.48           | 1.46     |
| PB030-2M | 54.1       | 7.59            | 11.65           | 1.53     |

Note: 1 kN = 0.225 kip; 1 mm = 0.039 in.

that the high ductility of specimens with vertical U-jackets was obtained at the expense of early yielding, and its overall deformation capacity was inferior to specimens with either mechanical plates or inclined U-jackets. It is indicated that  $\delta_y$  of specimens with vertical U-jackets were smaller than those of specimens with inclined U-jackets and mechanical plates,

as shown in Fig. 15(a), and  $\delta_u$  of specimens with vertical U-jackets were similar to those of specimens with inclined U-jackets and smaller than those of specimens with mechanical plates, as shown in Fig. 15(b). Because  $\delta_y$  serves as the denominator in the definition of  $\eta_D$ , it shows a greater influence on  $\eta_D$  than  $\delta_u$ . Therefore, the specimens with vertical U-jackets had the highest calculated ductility at the cost of early yielding.

#### THEORETICAL EVALUATION OF ULTIMATE LOAD

Based on existing analytic research<sup>12,39</sup> and experimental research,<sup>4</sup> a new theoretical model for evaluating the ultimate load of RC beams strengthened with fully or partially bonded CFRP and U-jacket anchorage (the influence of debonding is not considered in the proposed theoretical model) that fail due to CFRP IC debonding is proposed.

Chahrour and Soudki<sup>12</sup> suggested that for RC beams strengthened with bonded CFRP, the applied load can be calculated by Eq. (1)

$$M = \frac{\epsilon_c E_c b c^2}{3} + A_s f_y (h_s - c) + A_f E_f \epsilon_f (h - c) \quad (1)$$

where

$$c = \frac{2(A_s f_y + A_f E_f \epsilon_f)}{\epsilon_c E_c b} \quad (2)$$

In fact, from Eq. (1) and (2), the ultimate load of the specimens cannot be obtained directly because of the two unknown quantities,  $\epsilon_c$  and  $\epsilon_f$ . For given  $\epsilon_c$  and  $\epsilon_f$ , Eq. (1) and (2) yield the corresponding load of the specimen. In the original research by Chahrour and Soudki,<sup>12</sup>  $\epsilon_c$  and  $\epsilon_f$  were obtained through tests. However, to assess the beams in practice, it is necessary to make reasonable assumptions about these two values. In the case of evaluating the ultimate load, it can be assumed that concrete in the compression zone reaches its compressive strength, that is,  $\epsilon_c E_c = f_c$ . For  $\epsilon_f$ , Li and Wu<sup>39</sup> recommended a theoretical model to calculate the debonding strain of CFRP due to IC debonding

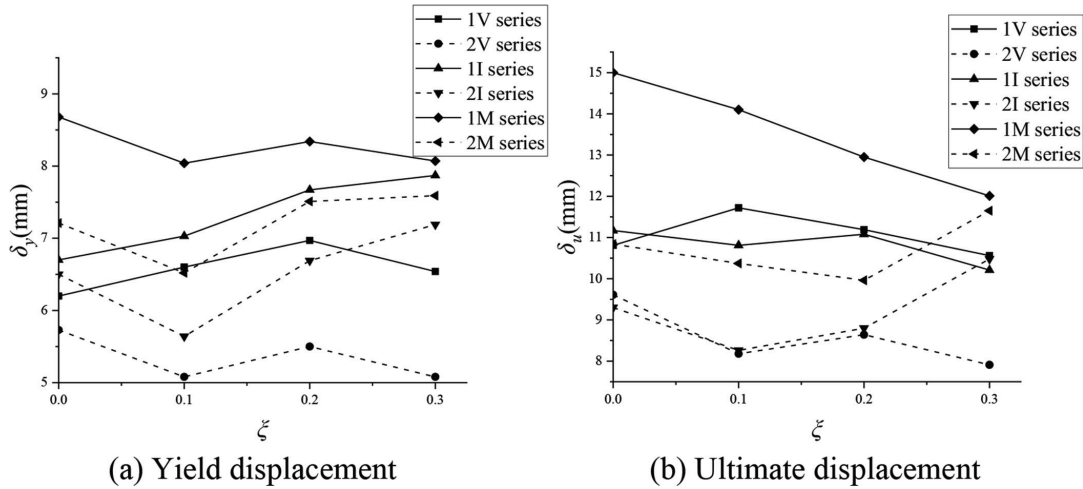


Fig. 15—Relationship between yield (ultimate) displacement and unbonded ratio. (Note: 1 mm = 0.039 in.)

$$\varepsilon_{fd} = \frac{\beta_w}{\sqrt{E_f t_f}} (0.427 f_c^{0.25} + 0.588 f_c^{0.3}) \quad (3)$$

where  $\varepsilon_{fd}$  is the debonding strain of CFRP;  $E_f$  is the elastic modulus of CFRP (MPa);  $t_f$  is the thickness of the CFRP sheet (mm);  $f_c$  is the cylinder compressive strength of concrete (MPa); and  $\beta_w = \sqrt{(2 - b_f/b)/(1 + b_f/b)}$ , where  $b_f$  and  $b$  are the width of the attached CFRP and beam, respectively.

To consider the effect of inclined U-jackets, it is assumed in this paper that the inclined U-jackets improve the performance of the beam by exerting an action on the bottom of the beam. Therefore, in Eq. (1) and (2), additional terms need to be added to represent the influence of inclined U-jackets, as follows

$$M_i = \frac{f_c b c_i^2}{3} + A_s f_y (h_s - c) + A_f E_f \varepsilon_{fd} (h - c_i) + 2 A_j E_f \varepsilon_{fd} (h - c_i) \cos \varphi \quad (4)$$

$$c_i = \frac{2(A_s f_y + A_f E_f \varepsilon_{fd} + 2 A_j E_f \varepsilon_{fd} \cos \varphi)}{b f_c} \quad (5)$$

where  $\varepsilon_{fd}$  is the strain of the CFRP U-jacket at debonding; and  $\varphi$  is the angle between the inclined U-jacket and horizontal plane: for vertical U-jacket specimens,  $\varphi = 90$  degrees.

Based on the experimental investigation by Fu et al.,<sup>4</sup> it is assumed that  $\varepsilon_{fd} = 0.2\varepsilon_u$ . The experimental results of U-jacket specimens in this study and collected from existing literature,<sup>4,40</sup> as well as corresponding calculated results, are listed in Table 5. It can be seen that  $P_{u,c}/P_{u,e}$  has a mean of 0.99, standard deviation of 0.09, and coefficient of variation of 0.09, which indicates a good agreement between the proposed model and the experimental results.

## CONCLUSIONS

This paper investigated the flexural properties of reinforced concrete (RC) beams strengthened with partially bonded carbon fiber-reinforced polymer (CFRP). A new parameter called the unbonded ratio was introduced to measure the degree of unbonded CFRP, which is defined as the ratio of unbonded length to the total length of the CFRP sheet. The

combined effects of partially bonded CFRP (unbonded ratio) and anchorage methods on the mechanical properties of RC beams strengthened with CFRP are investigated. Based on the experimental investigation and analysis of experimental results, the following conclusions can be drawn:

1. The results of the analysis indicate that the mechanical-plate anchorage-strengthened RC beam specimens show the highest ultimate load, followed by the inclined U-jacket and then the vertical U-jacket. Ultimate load decreased when the unbonded ratio increased in the pure bending zone and increased when the unbonded ratio approached the critical unbonded ratio.

2. It also shows that the cracking load was not affected by the unbonded ratio and the anchorage method, but increased significantly with the increasing number of CFRP layers.

3. The flexural stiffness of CFRP-strengthened RC beams was significantly influenced by the anchorage method. Inclined U-jacket anchorages increased stiffness the most effectively among the three anchorage methods, and the stiffness of specimens with mechanical plates was higher than that with vertical U-jackets.

4. It shows that the ductility of the test beams decreased with the increase in the number of CFRP layers and was significantly influenced by the anchorage method. The ductility of the specimens with vertical U-jackets was higher than that of specimens with mechanical plates, and the latter was higher than that of specimens with inclined U-jackets. However, specimens with vertical U-jackets yielded prematurely and had less overall capacity of deformation than specimens with mechanical-plate anchorage.

5. It exhibits that the crack width was not significantly affected by the unbonded ratio and anchorage method, but the crack propagation was restrained effectively by increasing the CFRP layers. All specimens showed similar crack patterns, except the two-layer specimens with vertical U-jackets, which had major shear cracks near supports.

6. A theoretical model for the ultimate load of RC beams strengthened with inclined U-jackets was proposed. The ratio of calculated to experimental result has a mean of 0.99, standard deviation of 0.09, and coefficient of variation

**Table 5—Ultimate loads of U-jacket specimens: values and comparison**

| Study                           | Specimen     | $P_{u,es}$ kN | $P_{u,cs}$ kN | $P_{u,c}/P_{u,e}$ |
|---------------------------------|--------------|---------------|---------------|-------------------|
| Present study                   | FB-1V        | 42.7          | 39.5          | 0.93              |
|                                 | FB-1I        | 51.6          | 44.1          | 0.85              |
|                                 | FB-2V        | 44.5          | 46.1          | 1.04              |
|                                 | FB-2I        | 56.9          | 50.5          | 0.89              |
|                                 | PB010-1V     | 44.4          | 40.8          | 0.92              |
|                                 | PB010-1I     | 47.6          | 45.4          | 0.95              |
|                                 | PB010-2V     | 44.2          | 47.4          | 1.07              |
|                                 | PB010-2I     | 50.5          | 51.8          | 1.03              |
|                                 | PB020-1V     | 44.6          | 40.8          | 0.91              |
|                                 | PB020-1I     | 49.6          | 45.4          | 0.92              |
|                                 | PB020-2V     | 47.3          | 47.4          | 1.00              |
|                                 | PB020-2I     | 54.0          | 51.8          | 0.96              |
|                                 | PB030-1V     | 44.8          | 40.8          | 0.91              |
|                                 | PB030-1I     | 48.8          | 45.4          | 0.93              |
| Fu et al. <sup>4</sup>          | PB030-2V     | 44.8          | 47.4          | 1.06              |
|                                 | PB030-2I     | 52.4          | 51.8          | 0.99              |
|                                 | I45W100H350  | 122.9         | 134.1         | 1.09              |
|                                 | I45W150H350  | 140.7         | 143.3         | 1.02              |
|                                 | I45W200H350  | 150.3         | 152.6         | 1.02              |
|                                 | I45W400H350  | 159.2         | 188.8         | 1.19              |
|                                 | I45W150H141  | 133.3         | 143.3         | 1.08              |
| Al-Saawani et al. <sup>40</sup> | V90W150H350  | 95.5          | 115.3         | 1.21              |
|                                 | I135W150H350 | 92.5          | 86.7          | 0.94              |
|                                 | 1U45W50L1    | 250.1         | 267.2         | 1.07              |
|                                 | 1U45W100L1   | 289.6         | 283.4         | 0.98              |
|                                 | 1U45W150L1   | 316.1         | 299.3         | 0.95              |
|                                 | 1U45W200L1   | 337.5         | 315.1         | 0.93              |
|                                 | 1U45W300L1   | 360.0         | 346.0         | 0.96              |
|                                 |              | Mean          | 0.99          |                   |
|                                 |              | S.D.          | 0.08          |                   |
|                                 |              | C.V.          | 0.08          |                   |

Note: S.D. is standard deviation; C.V. is coefficient of variation. 1 kN = 0.225 kip.

of 0.09, which indicates a good agreement between the proposed model and the tests.

### AUTHOR BIOS

**Qi Cao** is an Associate Professor at Dalian University of Technology, Dalian, Liaoning, China. He received his MS from Washington State University, Pullman, WA, and his PhD from the University of Tennessee, Knoxville, TN. His research interests include fiber-reinforced polymer (FRP)-reinforced and strengthened concrete structures.

**Xingchao Wang** is a Graduate Student at Dalian University of Technology, where he received his BS and MS. His research interests include FRP and steel-plate composite walls.

**Zhimin Wu** is a Professor at Dalian University of Technology, where he received his PhD. His research interests include fracture mechanics of concrete.

**Rongxiong Gao** is a Professor at Huazhong University of Science and Technology, Wuhan, Hubei, China. He received his PhD from Wuhan University of Technology, Wuhan, Hubei, China. His research interests include bridge engineering and FRP rehabilitation and repair in bridges.

**Xin Jiang** is a Professor at Wuhan Institute of Technology, Wuhan, Hubei, China. He received his MS from Changsha University of Science and Technology, Changsha, Hunan, China, and his PhD from the University of Tennessee, Knoxville. His research interests include bridge analysis and FRP.

### ACKNOWLEDGMENTS

This work is supported by the National Natural Science Foundation of China (Grant No. 52271264) and the Natural Science Foundation of Liaoning Province (Project No. 2021-MS-129).

### NOTATION

$A_f, A_j, A_s$  = cross-section area of CFRP sheet, CFRP U-jacket (one side), and longitudinal steel bars, respectively  
 $b, b_f$  = width of beam and CFRP sheet, respectively  
 $c, c_i$  = location of neutral axis without and with inclined U-jacket, respectively  
 $E_c, E_f$  = elastic modulus of concrete and CFRP, respectively  
 $f_c, f_y$  = compressive strength of concrete and yield strength of longitudinal steel bars, respectively  
 $h, h_s$  = height of beam and location of longitudinal steel bars, respectively  
 $L_f, L_{pb}$  = length of attached CFRP sheet and pure bending zone, respectively  
 $M, M_i$  = bending moment without and with inclined U-jacket, respectively  
 $P, P_{cr}, P_u$  = applied load, cracking load, and ultimate load, respectively  
 $P_{u,es}, P_{u,c}$  = experimental and calculated ultimate load, respectively  
 $w_{cr}$  = crack width  
 $x$  = unbonded length  
 $\delta, \delta_y, \delta_u$  = displacement, yield displacement, and ultimate displacement at midspan, respectively  
 $\epsilon_c, \epsilon_f$  = strain of concrete in compression face and attached CFRP, respectively  
 $\epsilon_{fd}, \epsilon_{jd}$  = debonding strain of attached CFRP sheet and strain of U-jacket when IC debonding failure occurs, respectively  
 $\eta_D$  = displacement ductility index  
 $\phi$  = angle between inclined U-jacket and horizontal plane  
 $\xi$  =  $x/L_f$ , unbonded ratio  
 $\xi_{cr}$  =  $L_{pb}/L_f$ , critical unbonded ratio

### REFERENCES

- Cao, Q., and Ma, Z. J., "Behavior of Externally Fiber-Reinforced Polymer Reinforced Shrinkage-Compensating Concrete Beams," *ACI Structural Journal*, V. 108, No. 5, Sept.-Oct. 2011, pp. 592-600.
- Dai, J.-G.; Gao, W. Y.; and Teng, J. G., "Bond-Slip Model for FRP Laminates Externally Bonded to Concrete at Elevated Temperature," *Journal of Composites for Construction*, ASCE, V. 17, No. 2, Apr. 2013, pp. 217-228. doi: 10.1061/(ASCE)CC.1943-5614.0000337
- Zhang, S. S.; Teng, J. G.; and Yu, T., "Bond Strength Model for CFRP Strips Near-Surface Mounted to Concrete," *Journal of Composites for Construction*, ASCE, V. 18, No. 3, June 2014, p. A4014003. doi: 10.1061/(ASCE)CC.1943-5614.0000402
- Fu, B.; Tang, X. T.; Li, L. J.; Liu, F.; and Lin, G., "Inclined FRP U-Jackets for Enhancing Structural Performance of FRP-Plated RC Beams Suffering from IC Debonding," *Composite Structures*, V. 200, Sept. 2018, pp. 36-46. doi: 10.1016/j.compstruct.2018.05.074
- Ye, H.; Zhang, Q.; Liu, C.; Wu, C.; and Duan, Z., "Failure Mechanisms Governing Anchoring Force of Friction-Based Wedge Anchorage for Prestressed CFRP Plate," *Composite Structures*, V. 225, Oct. 2019, Article No. 111142. doi: 10.1016/j.compstruct.2019.111142
- Lu, X. Z.; Teng, J. G.; Ye, L. P.; and Jiang, J. J., "Intermediate Crack Debonding in FRP-Strengthened RC Beams: FE Analysis and Strength Model," *Journal of Composites for Construction*, ASCE, V. 11, No. 2, Apr. 2007, pp. 161-174. doi: 10.1061/(ASCE)1090-0268(2007)11:2(161)
- Cao, Q.; Zhou, J.; Wu, Z.; and Ma, Z. J., "Flexural Behavior of Prestressed CFRP Reinforced Concrete Beams by Two Different Tensioning Methods," *Engineering Structures*, V. 189, June 2019, pp. 411-422. doi: 10.1016/j.engstruct.2019.03.051
- Zhou, A.; Qin, R.; Feo, L.; Penna, R.; and Lau, D., "Investigation on Interfacial Defect Criticality of FRP-Bonded Concrete Beams,"

*Composites Part B: Engineering*, V. 113, Mar. 2017, pp. 80-90. doi: 10.1016/j.compositesb.2016.12.055

9. Burgoyne, C. J., "Should FRP be Bonded to Concrete?" *Fiber-Reinforced-Plastic Reinforcement for Concrete Structures – International Symposium*, SP-138, A. Nanni and C. W. Dolan, eds., American Concrete Institute, Farmington Hills, MI, 1993, pp. 367-380.

10. Lees, J. M., and Burgoyne, C. J., "Experimental Study of Influence of Bond on Flexural Behavior of Concrete Beams Pretensioned with Aramid Fiber Reinforced Plastics," *ACI Structural Journal*, V. 96, No. 3, May-June 1999, pp. 377-385.

11. Lees, J. M., and Burgoyne, C. J., "Analysis of Concrete Beams with Partially Bonded Composite Reinforcement," *ACI Structural Journal*, V. 97, No. 2, Mar.-Apr. 2000, pp. 252-258.

12. Chahrouh, A., and Soudki, K., "Flexural Response of Reinforced Concrete Beams Strengthened with End-Anchored Partially Bonded Carbon Fiber-Reinforced Polymer Strips," *Journal of Composites for Construction*, ASCE, V. 9, No. 2, Apr. 2005, pp. 170-177. doi: 10.1061/(ASCE)1090-0268(2005)9:2(170)

13. Choi, H. T.; West, J. S.; and Soudki, K. A., "Analysis of the Flexural Behavior of Partially Bonded FRP Strengthened Concrete Beams," *Journal of Composites for Construction*, ASCE, V. 12, No. 4, Aug. 2008, pp. 375-386. doi: 10.1061/(ASCE)1090-0268(2008)12:4(375)

14. Qi, L.; Yang, Y.; Zhang, Z.; and Zhang, Y., "Experiment and Study on RC Beams Strengthened by Bonding CFRP Partially," *Highway*, No. 10, 2007, pp. 21-26. (in Chinese)

15. Zhang, Z.; Qi, L.; and Zhang, Y., "Experiment and Study on Normal Section of RC Beams Strengthened by Bonding CFRP Partially," *Railway Engineering*, No. 11, 2007, pp. 17-19. (in Chinese)

16. Yin, J., "Study on Ductility of Reinforced Concrete Flexural Members Strengthened with Partially Bonded CFRP," master's dissertation, Anhui University of Science and Technology, Huainan, Anhui, China, 2017. (in Chinese)

17. Zhang, Z., and Yin, J., "Effect of Mid-Span Blank Bonding Length on Mechanical Properties of Beams Strengthened by CFRP," *Journal of Henan University of Engineering*, V. 33, No. 4, 2021, pp. 26-30, 47. (in Chinese)

18. Zhang, Z., and Huang, Q., "Study on Flexural Behavior of Partially Bonded FRP Strengthened RC Beams," *Journal of Railway Science and Engineering*, V. 17, No. 4, 2022, pp. 965-971. (in Chinese)

19. ACI Committee 440, "Guide for the Design and Construction of Externally Bonded FRP Systems for Strengthening Concrete Structures (ACI 440.2R-17)," American Concrete Institute, Farmington Hills, MI, 2017, 112 pp.

20. Siddika, A.; Al Mamun, M. A.; Alyousef, R.; and Amran, Y. H. M., "Strengthening of Reinforced Concrete Beams by Using Fiber-Reinforced Polymer Composites: A Review," *Journal of Building Engineering*, V. 25, Sept. 2019, Article No. 100798. doi: 10.1016/j.jobbe.2019.100798

21. Zaki, M. A., and Rasheed, H. A., "Behavior of Reinforced Concrete Beams Strengthened Using CFRP Sheets with Innovative Anchorage Devices," *Engineering Structures*, V. 215, July 2020, Article No. 110689. doi: 10.1016/j.engstruct.2020.110689

22. Al-Rousan, R., and Al-Saraiheh, S., "Impact of Anchored Holes Technique on Behavior of Reinforced Concrete Beams Strengthened with Different CFRP Sheet Lengths and Widths," *Case Studies in Construction Materials*, V. 13, Dec. 2020, Article No. e00405. doi: 10.1016/j.cscm.2020.e00405

23. Ekenel, M.; Rizzo, A.; Myers, J. J.; and Nanni, A., "Flexural Fatigue Behavior of Reinforced Concrete Beams Strengthened with FRP Fabric and Pre-cured Laminate Systems," *Journal of Composites for Construction*, ASCE, V. 10, No. 5, Oct. 2006, pp. 433-442. doi: 10.1061/(ASCE)1090-0268(2006)10:5(433)

24. Dong, K.; Ji, Z.; Yang, S.; Du, D.; and Liu, Y., "Experimental Study on Bearing Capacity of FRP-Concrete Bonding Interface with Mechanical End Anchorage," *Journal of Building Structures*, V. 41, No. S1, 2020, pp. 399-405. (in Chinese)

25. Mostofinejad, D.; Hosseini, S. M.; Nader Tehrani, B.; Eftekhari, M. R.; and Dyari, M., "Innovative Warp and Wool Strap (WWS) Method

to Anchor the FRP Sheets in Strengthened Concrete Beams," *Construction and Building Materials*, V. 218, Sept. 2019, pp. 351-364. doi: 10.1016/j.conbuildmat.2019.05.117

26. Fu, B.; Chen, G. M.; and Teng, J. G., "Mitigation of Intermediate Crack Debonding in FRP-Plated RC Beams Using FRP U-Jackets," *Composite Structures*, V. 176, Sept. 2017, pp. 883-897. doi: 10.1016/j.compstruct.2017.05.049

27. Mostofinejad, D., and Mahmoudabadi, E., "Grooving as Alternative Method of Surface Preparation to Postpone Debonding of FRP Laminates in Concrete Beams," *Journal of Composites for Construction*, ASCE, V. 14, No. 6, Dec. 2010, pp. 804-811. doi: 10.1061/(ASCE)CC.1943-5614.0000117

28. Mostofinejad, D., and Tabatabaei Kashani, A., "Experimental Study on Effect of EBR and EBROG Methods on Debonding of FRP Sheets Used for Shear Strengthening of RC Beams," *Composites Part B: Engineering*, V. 45, No. 1, Feb. 2013, pp. 1704-1713. doi: 10.1016/j.compositesb.2012.09.081

29. Hosseini, A., and Mostofinejad, D., "Experimental Investigation into Bond Behavior of CFRP Sheets Attached to Concrete Using EBR and EBROG Techniques," *Composites Part B: Engineering*, V. 51, Aug. 2013, pp. 130-139. doi: 10.1016/j.compositesb.2013.03.003

30. Mostofinejad, D., and Moghaddas, A., "Bond Efficiency of EBR and EBROG Methods in Different Flexural Failure Mechanisms of FRP Strengthened RC Beams," *Construction and Building Materials*, V. 54, Mar. 2014, pp. 605-614. doi: 10.1016/j.conbuildmat.2014.01.002

31. Mostofinejad, D., and Akhlaghi, A., "Experimental Investigation of the Efficacy of EBROG Method in Seismic Rehabilitation of Deficient Reinforced Concrete Beam-Column Joints Using CFRP Sheets," *Journal of Composites for Construction*, ASCE, V. 21, No. 4, Aug. 2017, p. 04016116. doi: 10.1061/(ASCE)CC.1943-5614.0000781

32. Mashrei, M. A.; Makki, J. S.; and Sultan, A. A., "Flexural Strengthening of Reinforced Concrete Beams Using Carbon Fiber Reinforced Polymer (CFRP) Sheets with Grooves," *Latin American Journal of Solids and Structures*, V. 16, No. 4, 2019, Article No. e176. doi: 10.1590/1679-78255514

33. Cao, Q.; Tao, J.; Ma, Z. J.; and Wu, Z., "Axial Compressive Behavior of CFRP-Confined Expansive Concrete Columns," *ACI Structural Journal*, V. 114, No. 2, Mar.-Apr. 2017, pp. 475-485. doi: 10.14359/51689450

34. GB/T 50081-2019, "Standard for Test Methods of Concrete Physical and Mechanical Properties," Ministry of Housing and Urban-Rural of the People's Republic of China, Beijing, China, 2019, 103 pp. (in Chinese)

35. GB/T 3354-1999, "Test Method for Tensile Properties of Oriented Fiber Reinforced Plastics," General Administration of Quality Supervision, Inspection and Quarantine of the People's Republic of China, Beijing, China, 1999, 4 pp. (in Chinese)

36. GB/T 228.1-2010, "Metallic Materials – Tensile Testing – Part 1: Method of Test at Room Temperature," General Administration of Quality Supervision, Inspection and Quarantine of the People's Republic of China, Beijing, China, 2010, 61 pp. (in Chinese)

37. Teng, J. G., and Chen, J. F., "Mechanics of Debonding in FRP-Plated RC Beams," *Proceedings of the Institution of Civil Engineers - Structures and Buildings*, V. 162, No. 5, Oct. 2009, pp. 335-345. doi: 10.1680/stbu.2009.162.5.335

38. Park, R., "State-of-the Art Report: Ductility Evaluation from Laboratory and Analytical Testing," *Proceedings of the Ninth World Conference on Earthquake Engineering (9WCEE)*, V. 8, Tokyo-Kyoto, Japan, Aug. 1988, pp. 605-616.

39. Li, X.-H., and Wu, G., "Finite-Element Analysis and Strength Model for IC Debonding in FRP-Strengthened RC Beams," *Journal of Composites for Construction*, ASCE, V. 22, No. 5, Oct. 2018, p. 04018030. doi: 10.1061/(ASCE)CC.1943-5614.0000863

40. Al-Saawani, M. A.; El-Sayed, A. K.; and Al-Negheimish, A. I., "Inclined FRP U-Wrap Anchorage for Preventing Concrete Cover Separation in FRP Strengthened RC Beams," *Arabian Journal for Science and Engineering*, V. 48, No. 4, Apr. 2023, pp. 4879-4892.